RSC Advances

PAPER

View Article Online
View Journal | View Issue

Cite this: *RSC Adv.*, 2022, **12**, 33955

Necked gold nanoparticles prepared by submerged alternating current arc discharge in water

K. Jankowski, *[ab] J. Jabłońska,[ac] P. Uznański,[b] S. Całuch,[a] M. Szybowicz,[c] R. Brzozowski,[b] A. Ostafin,[a] M. Kwaśny[d] and M. Tomasik[a]

The article presents the method of producing gold nanoparticles using a high voltage arc discharge of alternating current with a frequency of 50 Hz in distilled water. The equipment necessary to carry out the process is described, including the construction of the reactor and the power source of a very simple design necessary to generate a high-voltage arc discharge between the electrodes. Arc discharge processes were carried out two times for 2 and 5 minutes, respectively, in ambient conditions without thermostating the reactor, at medium temperature varying in the range of 25–70 °C. The obtained gold nanoparticles were examined by means of various analytical techniques such as UV-vis spectroscopy, zeta potential measurement, energy dispersive X-ray analysis (EDS), X-ray diffraction (XRD). The morphology, surface, and size of the obtained nanoparticles were carried out using transmission electron microscopy (HRTEM) and dynamic light scattering (DLS). The concentration of the obtained colloids were determined using the mass spectrometry ICP-MS technique. The results show that high-voltage AC arc discharge is a simple and effective way to obtain stable gold nanoparticles under environmentally friendly conditions at relatively low production costs, and can be considered as an alternative to arc discharge nanoparticles synthesis by means of direct current (DC) methods.

Received 25th September 2022
Accepted 21st November 2022

DOI: 10.1039/d2ra06050g

rsc.li/rsc-advances

1. Introduction

Metal nanoparticles have been of great interest since Turkevich's[1] pioneering work on the nucleation and growth of colloidal gold using an electron microscope. Another milestone in the synthesis of gold nanoparticles of significant importance in the development of nanoscience was Brust's work from 1994,[2] which inspired research in various fields of optics, optoelectronics, catalysis, medicine, biosensors, and so on. For example, gold nanoparticles are successfully used in biomedicine. The high surface-to-volume ratio of gold nanoparticles makes it possible to cover their surface with many compounds of functional importance. Their various new features have found many applications *e.g.* in biosensors to detect sugars,[3] nucleotides,[4] DNA,[4] proteins,[5] toxins,[6] viruses.[7] The possibility of obtaining different shapes of nanoparticles and structure increases their attractiveness in sensing phenomena. The operation of sensors with the use of gold nanoparticles is based on a variety of analytical techniques: colorimetry, *i.e.* colour changes of nanoparticles after aggregation,[8] fluorescence, or SERS spectroscopy.[9] Gold nanoparticles are also applied as catalysts in chemical reactions,[10] as conductors in electronics,[11] and as probes for biological imaging.[12]

The most commonly known approaches of producing gold nanoparticles are bottom-up methods involving the chemical reduction of organometallic precursors and salts of gold compounds,[13–18] or physical reduction including UV radiolysis,[18,19] ultrasound,[20] or electron beam lithography.[21,22] In turn pure physical top-down methods for the synthesis of metallic nanoparticles are based on bulk materials and use for synthesis *e.g.* laser ablation,[23,24] or electrical discharges,[25–28] and are among the methods that give less defined nanostructures due to the inability to control, on demand, the particle shape, size and size distribution on which their surface properties significantly depend.[29] On the other hand physical methods are powerful for producing nanoparticle colloids with a good stability despite the absence of organic stabilizers. Thus using these methods it is possible to successfully obtain pure gold nanoparticles with low toxicity[30,31] and very good biocompatibility.[32]

To meet the demand of necked gold nanoparticles motivates the development of different synthesis methods which have their own advantages and drawbacks. Arc discharge in liquids using direct current (DC) method,[33–35] appeared in the 1990s, was based on the production of graphite nanostructures.[36] One of its main advantages relies on its relative simplicity since it is based on a current flow between two solid electrodes in a liquid

[a]*Institute of Nanotechnology and Nanobiology, Jacob of Paradies University, Chopina St. 52, Bldg. 6, 66-400 Gorzow Wielkopolski, Poland. E-mail: kjankowski@ajp.edu.pl*
[b]*Centre of Molecular and Macromolecular Studies, Polish Academy of Sciences, Sienkiewicza 112 St., 90-363 Lodz, Poland*
[c]*Faculty of Materials Engineering and Technical Physics, Poznan University of Technology, Piotrowo 3A St., 61-138 Poznan, Poland*
[d]*Institute of Optoelectronics, Military University of Technology, Kaliskiego 2 St., 00-908 Warsaw, Poland*

environment. The ease of the apparatus construction, low concentration of the introduced impurities during synthesis, no need to use vacuum and a high yield make it attractive in applications also when scaling up for mass production.

Our studies have shown that alternating current (AC) arc discharge in water can be successfully used as an effective method of obtaining metal nanoparticles, and is a good alternative to DC arc discharge requiring the use of rectifying and filtering systems for the electrical signal. In the case of using an alternating current discharge with a frequency of 50 Hz, a system consisting of a transformer from the microwave oven (MOT) and an autotransformer for voltage regulation on the secondary winding MOT.[37] The described solution has also been successfully used for the preparation of silver nanoparticles and the production of elongated carbon wires.[36,38] Such a solution is relatively cheap, energy-efficient and environmentally friendly. Well-separated gold nanoparticles in pure water seem to be thermodynamically stable for a long time.

2. Materials and methods

2.1. Materials

Wires of 2 mm in diameter and 26 mm long for the top and bottom electrode were made from investment gold (99.9%, Heraeus). The process was carried out in distilled water with a conductivity of 0.55 μS and pH = 6.5. Acid, 0.1 M HCl purchased from Sigma Aldrich was used to etch the electrodes before electrolysis.

2.2. Analytical methods

Gold electrodes were weighed before and after the process using an electronic analytical balance AXIS ALN120 (Axis Sp. Zoo. Gdansk, Poland). Voltage values were measured with the use of a Fluke high-voltage probe (80K-6) and current values with a Hantek CC650 AC/DC clamp probe. The signals were monitored with a Tektronix TDS2024B oscilloscope and measurement data was collected *via* a USB port. Absorbance spectra of colloidal samples were measured in the range of 200–900 nm, using a Shimadzu 1240 UV-vis spectrophotometer with distilled water as a reference. The hydrodynamic diameter (D_h), by intensity, and zeta potential (Z) of gold particles were determined by dynamic light scattering (DLS) method, using Zeta-Sizer Nano ZS90 (Malvern Instruments, UK) equipped with HeNe red laser (λ = 633 nm) and at a measurement angle of 173°. X-ray diffraction (XRD) analysis was conducted on a Malvern Panalytical Aeris at the θ–2θ accusation scan with monochromatic Cu K_α radiation (λ = 1.5406 Å) operated at 40 kV and 7.5 mA. The scanning was done in the 2θ range of 20°–90°. Morphology, shape, and size of the gold nanoparticles were examined by the TEM technique with a FEI Titan 300 kV FEG TEM/STEM equipped with an EDAX EDS detector. Energy dispersive X-ray spectra (EDS) were obtained using a scanning electron microscope (SEM) JSM-6010LV/LA equipped with a silicon EDS detector. Elements were detected at accelerating voltage of 15–30 kV in high-vacuum mode. Colloids concentrations were measured using inductively coupled plasma mass spectrometry (ICP-MS) with a PerkinElmer ELAN DRC II spectrometer. Test samples were prepared by 10^4-fold dilution of the originally prepared samples to a volume of 50 mL. Inorganic Ventures 10 ppm gold (Au) ICP calibration/quality control standard with concentrations of 0.1, 1, 10, 50% and volumes of 50 mL was used to prepare the calibration curve.

2.3. Reactor system

The processes were carried out for 2 minutes (AuNPs-2) and 5 minutes (AuNPs-5), respectively. The preparation of gold nanoparticles in water took place in the reactor presented in Fig. 1a, which consists of a quartz tube with the length of 100 mm and a diameter of 80 mm, and Teflon covers sealed with O-rings. Each cover has a lead for the holders that clamp the gold electrodes. The clamp holders are connected to electric power supply. The toc electrode has an adjusting screw. This solution allows to control a correct distance of the electrodes necessary for ignition and continuous operation of the electric arc. The arc discharge for the electrical parameters used in this experiments occurs for a distance of 1.2 mm between the electrodes. There is a valve in the bottom cover that allows the reactor to be quickly emptied from the obtained colloid. The power supply system (Fig. 1b) that enables the generation of a continuous operation of an alternating voltage electric arc consists of an autotransformer and a microwave oven transformer (MOT) (Samsung DE26-00122B Microwave High-Voltage Transformer). The autotransformer controls low voltage in the range of 0–230 V, while the MOT transformer induces a 10-fold increase in the voltage obtained on the secondary winding, *e.g.* setting the autotransformer to 100 V, the MOT output will be 1000 V. The described power supply system operates with a mains frequency of 50 Hz. The voltage and current measurements during the process were made with the use of multifunction meters. For reasons of work safety and ensuring constant thermodynamic parameters, the MOT transformer was placed in a plastic container and poured over with transformer oil. All production processes were carried out at room temperature (21 °C) without cooling the reactor.

2.4. Submerged arc discharge process

Before the process, the gold electrodes were etched in 50 ml of 0.1 M HCl for 10 min at temperature 21 °C, and then rinsed copiously in distilled water. Dry electrodes were weighed before and after the arc discharge process. The total weight loss of the electrodes was 0.0044 g and 0.0063 g for AuNPs-2 and AuNPs-5, respectively. The assembled reactor equipped with Au electrodes and magnetic stirrer was filled with 160 mL of distilled water. The distance between the electrodes was set at 1.2 mm and a voltage of 1.5 kV from the secondary winding of the MOT transformer was applied to the electrodes. During arc discharge, the average voltage across the electrodes decreased to 1.25 kV (2.5 kV peak-to-peak voltage), and the current peak-to-peak was 0.85 A (Fig. 1c).

Experiments were conducted without reactor cooling. The temperature of the colloid after the 2 minutes process was 56 ± 3 °C, while after 5 minutes discharge it was 67 ± 3 °C. The

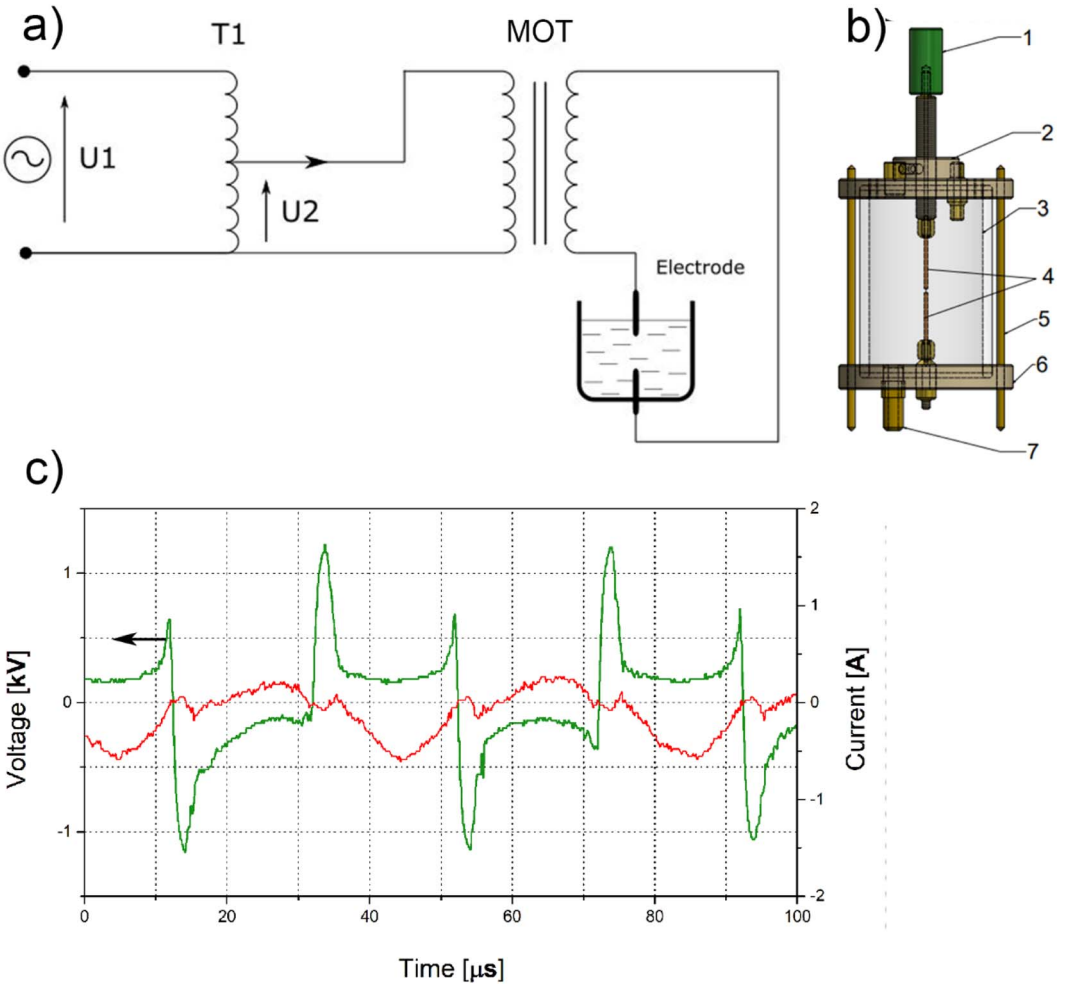

Fig. 1 (a) Diagram of a submerged continuous arc discharge reactor. (1) Adjusting screw, (2) top cover with gas dosing valve and first electrode clamp. (3) Borosilicate glass tube filled with water. (4) Wire gold electrodes (5) bottom cover with holder for the second electrode. (b) Scheme of power supply. (c) Current–voltage characteristic during AC arc discharge.

colloids were allowed to cool down to room temperature prior to analysis.

3. Results and discussion

3.1. UV-vis spectroscopy

The Au nanoparticles concentration was controlled by the arc discharge time, which in the present study was 2 and 5 minutes, respectively, for AuNPs-2 and AuNPs-5 colloid. Formation of gold nanoparticles during the AC arc process was followed by change in the water colour (inset Fig. 2) of the reaction solution from colourless by pink (AuNPs-2) to dark purple (AuNPs-5). The UV-vis absorption spectra of the AuNPs with different concentrations are shown in Fig. 2. The clearly visible broad band with a maximum at 525 nm for AuNPs-2 derives from the phenomenon of surface plasmon resonance (SPR) and is an inherent feature of gold nanoparticles.[39] For the second sample, AuNPs-5, the spectrum position slightly shifts to 536 nm and gains intensity at ~600 nm. The shape of the band with long absorption tail suggests the presence of not only spherical nanoparticles in the water but objects of irregular shapes or aggregates.

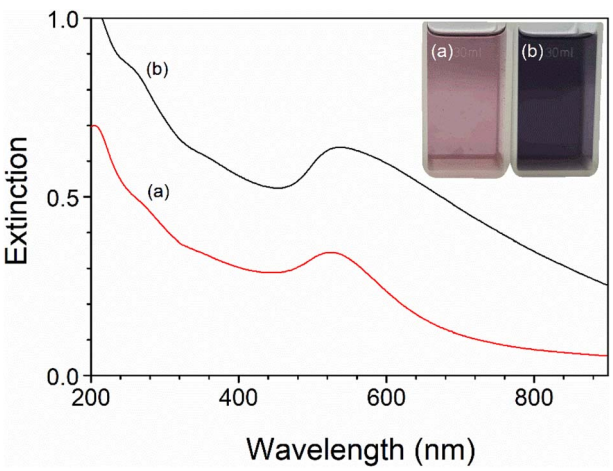

Fig. 2 UV-vis absorption spectra of gold nanoparticles of various concentrations obtained in the 2 minutes (AuNPs-2) and 5 minutes (AuNPs-5) high voltage AC arc process, measured in a cuvette with an optical path length of 1 mm. Inset: images of gold colloids AuNPs-2 (a) and AuNPs-5 (b).

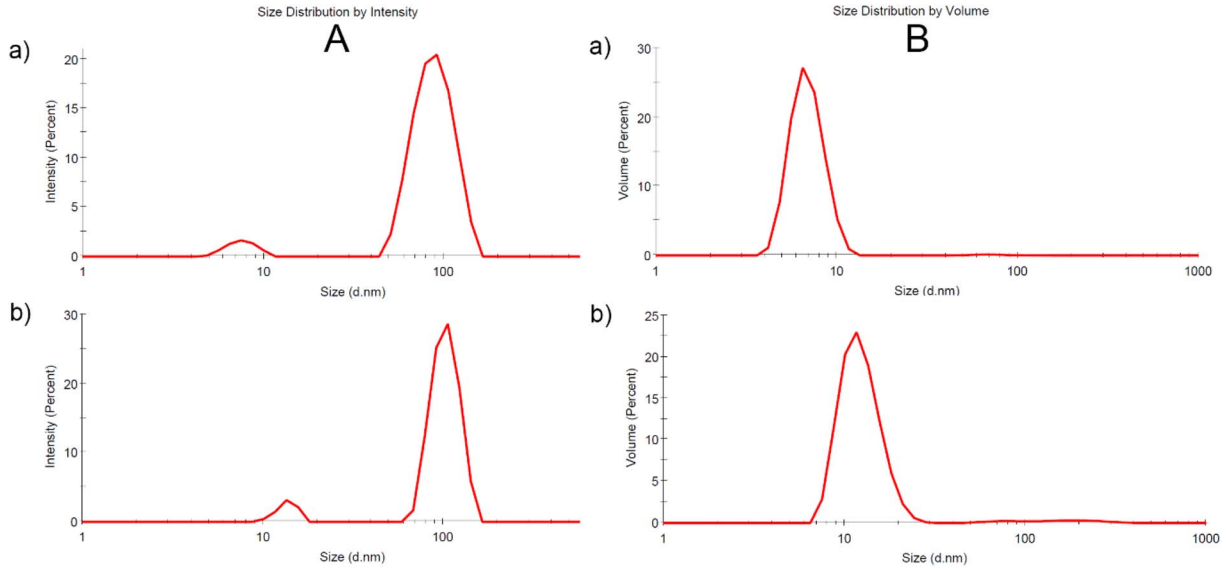

Fig. 3 Size distribution signals from measurements of dynamic light scattering by intensity (A) and volume (B) for AuNPs-2 (a) and AuNPs-5 (b) colloid. All signals are averaged from three repeat measurements.

3.2. Dynamic light scattering and zeta potential measurements

The size distribution profile of the produced gold nanoparticles measured by DLS method in terms of scattering intensity (A) and volume (B) is shown in Fig. 3a and b for samples AuNPs-2 and AuNPs-5, respectively. Although DLS only measures the hydrodynamic diameter of particles this technique directly represents the sizes in a native colloidal system. The scattered signals confirm the broad particle size distribution which agrees well with the UV-vis extinction profile extending into the

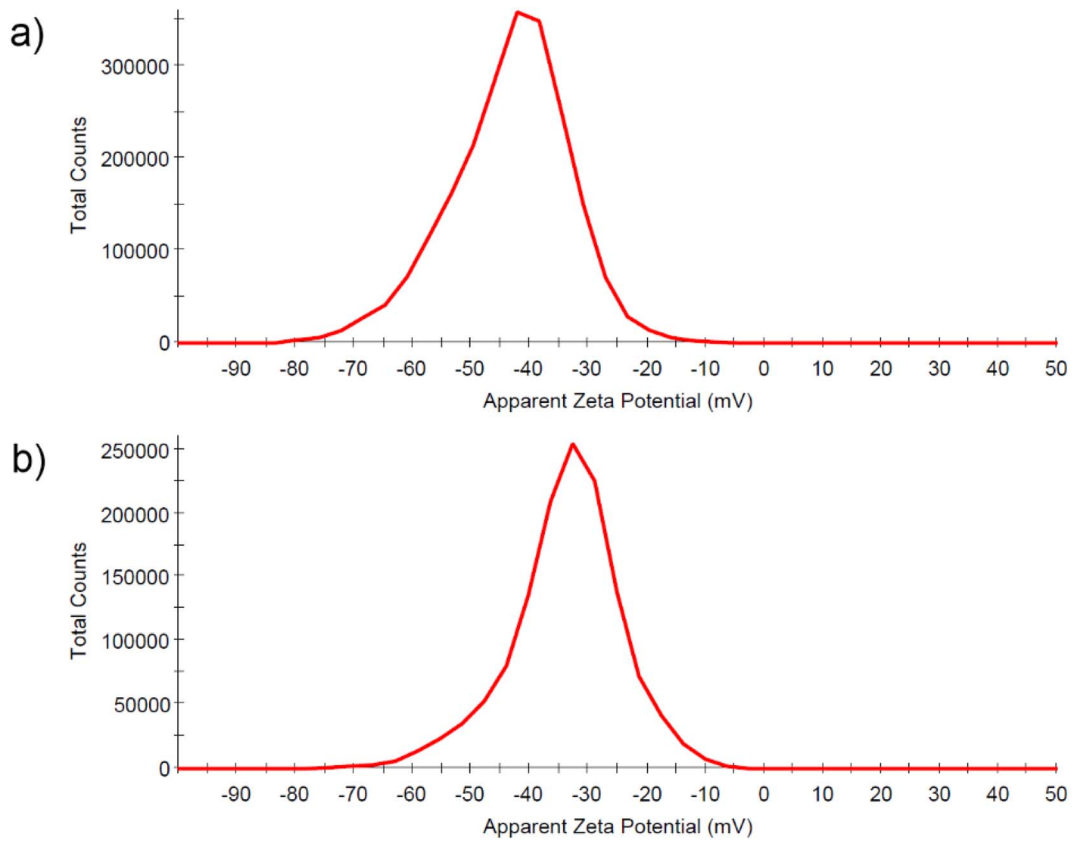

Fig. 4 Results of zeta potential measurements for the 2 minutes (a) and 5 minutes process (b).

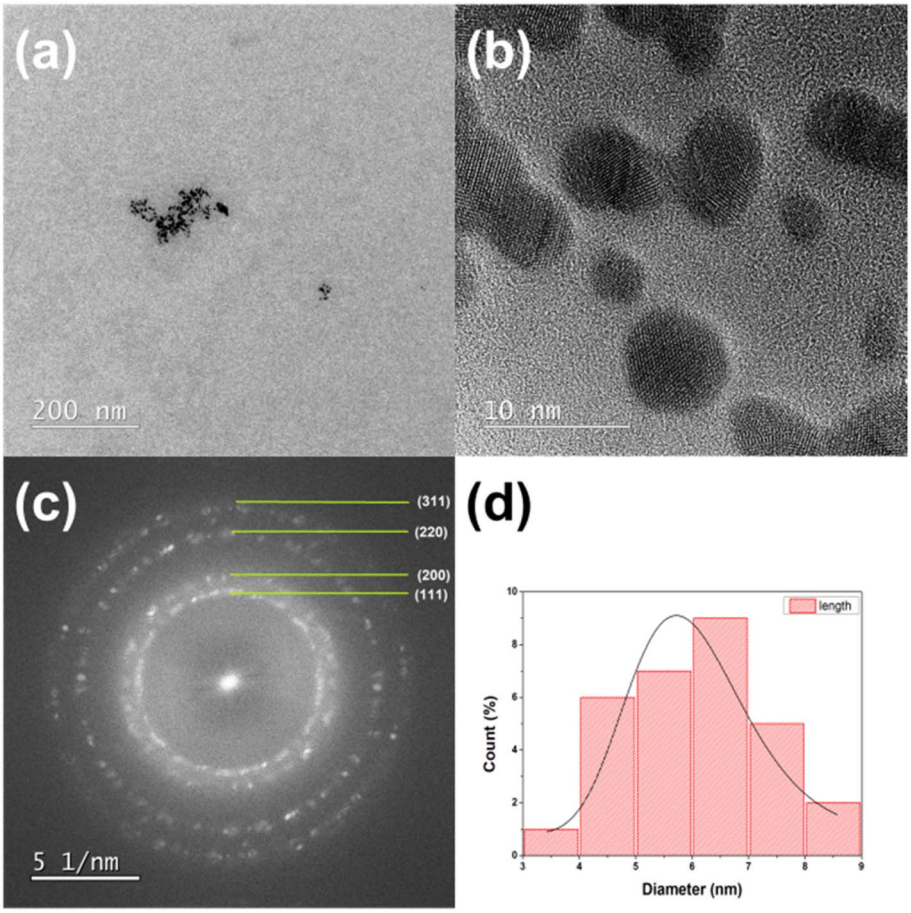

Fig. 5 TEM (a) and HRTEM (b) images, (c) SAED diffraction pattern, and (d) size distribution of AuNPs-2 nanoparticles obtained in the 2 minutes arc discharge process.

long-wavelength region. Size distribution profiles by scattering intensity reveal two NPs populations for both samples with an overall *z*-average size around 7.6 nm and 89.2 nm, for AuNPs-5, and around 13.6 nm and 103.4 nm, for AuNPs-5. This indicates that the sample consisted of aggregates. The size distribution by intensity of the DLS is skewed due to the 6^{th} power dependence of the light scattering intensity. The volume size distribution is more suitable for comparison with other volume based detection techniques such as UV-vis absorption. This is demonstrated in Fig. 3a and b (B) for colloid AuNPs-2 and AuNPs-5, respectively. As shown, the relative proportions of the two size distributions intensity convert to a particle size distribution by volume with a smaller average values, in this case 6.9 nm and 12.5 nm.

Zeta potential, which is the electrical potential at the sol interface was determined to be −43.5 mV for AuNPs-2, and −34.6 mV for AuNPs-5 (Fig. 4a and b). The Zeta potential provides information about the surface charge of the nanoparticles, which was negative here. Its value informs about the colloid's stability. The high negative zeta potential values are related to the electrostatic repulsive forces between the gold particles and make the colloid very stable for at least months, which was supported by the lack of changes in the UV-vis spectra and the value of the Zeta potential.

3.3. Transmission electron microscopy analysis

A transmission electron microscopy was used to verify the mean particle size and size distribution of gold nanoparticles. Fig. 5a and 6a show a typical TEM images of gold nanoparticles obtained from the discharge between pure gold electrodes in distilled water. These TEM images confirm the presence of polydispersed Au nanoparticles. The crystalline form of the obtained gold nanoparticles can be examined in the photos taken using the high resolution technique HRTEM (Fig. 5b and 6b). Selected area electron diffraction (SAED) analysis was used to determine lattice constants. The ring diffractograms are typical for polycrystalline samples where the diameter of each ring indicates interplanar distance of crystallographic planes. Thus the Scherrer ring patterns in Fig. 5c and 6c indicate the fcc gold structure with Miller indexes of (111), (200), (220), (311). Histograms plot describing the particle size distribution is shown in Fig. 5d and 6d. It is 5.7 nm for 2 minutes- and 8.4 nm for 5 minutes-process. By analyzing the TEM/HRTEM images and determining size distribution, we can conclude that

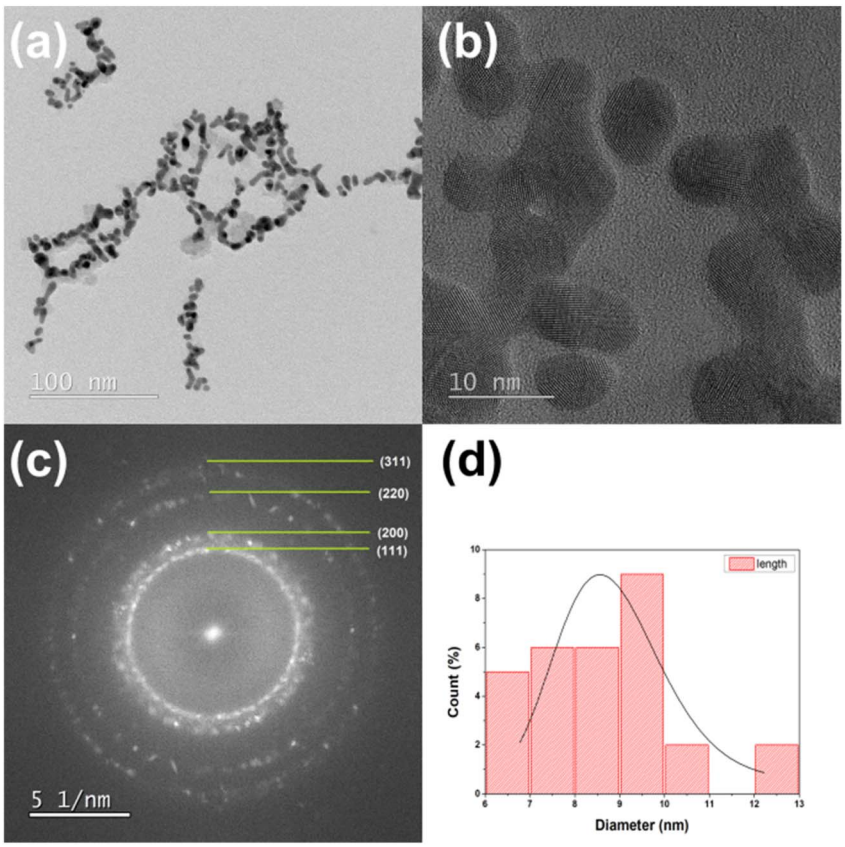

Fig. 6 TEM (a) and HRTEM (b) images, (c) SAED diffraction pattern, and (d) size distribution of AuNPs-5 nanoparticles from the 5 minutes arc discharge process.

a longer process causes an increase in size of the obtained gold nanoparticles. The AuNPs shape for the 5 minutes process are more irregular than for the 2 minutes process, nevertheless retaining its roundness.

3.4. X-ray diffraction (XRD) measurements

Fig. 7 shows XRD diffraction patterns for AuNPs-2 and AuNPs-5 samples along with maxima assigned according to the International Center Diffraction Data/Inorganic Crystal Structure Database (ICDD/ICSD Au reference code 00-004-0784 JCPDS file: 04-0784). Note that the (111) peak of gold is much more intense than the other existing Au diffraction peaks. There is a visible broadening of the diffraction peaks for both samples, indicating the presence of crystallites of reduced size. The broadening of an observed diffraction peak. Such a broadening can be characterized simplistically by its FWHM (full width at half maximum) value at a particular 2θ angle as 38°, 44°, 64°, 78°, and 82° respectively. Because the apparent FWHM of a peak is a mathematical combination (convolution) of the specimen broadening FWHM(S) and the instrumental broadening FWHM(I), the instrumental broadening is subtracted from that of the observed diffraction peak. If the crystallites (crystalline domains) in the specimen are free of lattice strain, their average size D can be estimated from the specimen broadening FWHM(S) of any single peak in the observed pattern according to the Scherrer formula:

$$D = K \times \lambda/(\mathrm{FWHM(S)} \times \cos(\theta))$$

where θ is the peak position and K is the dimensionless shape factor (for fcc lattice is assumed 0.94) of the average crystallite, λ is the X-ray wavelength, FWHM(S) is the line broadening at half the maximum intensity (FWHM), θ is the Bragg angle. The

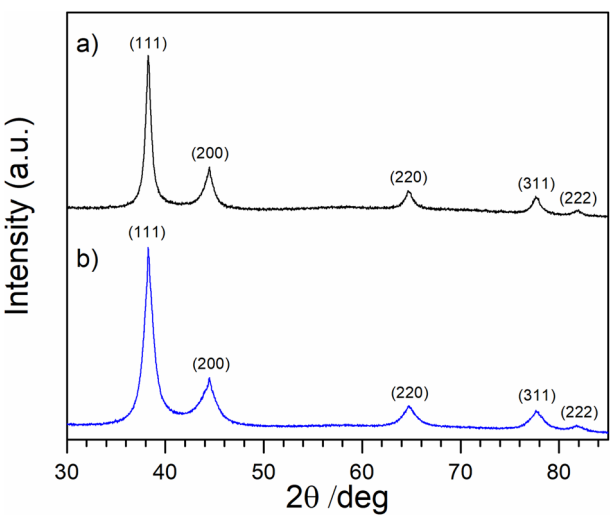

Fig. 7 XRD patterns of thin layers prepared by casting on a Si(510) zero diffraction substrate from AuNPs-2 (a) and AuNPs-5 (b) colloids.

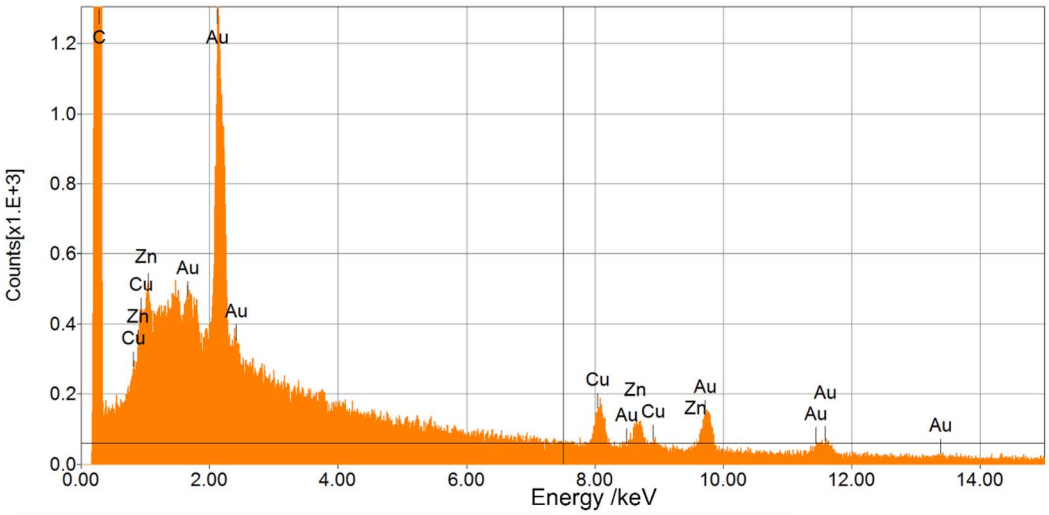

Fig. 8 EDS spectra of samples prepared from AuNPs-2 colloid.

calculated average crystallite sizes were 8.4 ± 3.2 and 11.6 ± 2.8 nm for AuNPs-2 and AuNPs-5 colloid, respectively. This means that the nanoparticles growing in the HV discharge arc are made of smaller crystallites.

3.5. Elemental analysis by energy dispersive X-ray spectroscopy (EDS)

EDS was used to determine which chemical elements were present in the sample and to estimate their relative abundance. Fig. 8 shows the EDS spectrum for AuNPs-2 (for AuNPs-5 is essentially similar). For both samples, the energy dispersive X-ray analysis of gold nanocrystallites showed a characteristic peak at approximately 2.2 keV (M_α), 9.71 keV ($L_{\beta1}$), 11.41 keV ($L_{\beta2}$), which corresponds to metallic gold. In the EDS spectrum, in both samples we can find peaks from such elements as C, Cu and Zn. The carbon is derived from the carbon strip covering the brass substrate (Cu and Zn) used in the SEM microscope. Differences in the intensity of a characteristic X-ray Au peaks can also be observed for different discharge time. It is clearly visible that the Au plasmon peak for the AuNPs-5 is more intense. It can therefore be concluded that the concentration of gold increases with the duration of the process.

3.6. ICP-MS and electrode weight loss measurements

Inductively coupled plasma mass spectrometry (ICP-MS) is a technique in which the composition of elements in a sample (mostly water-dissolved) can be determined using plasma and a spectrometer in concentrations as low as one part in 10^{15}. This is achieved by ionization in an inductively coupled plasma, and then using a mass spectrometer to determine the amount of ions. The Table 1 below shows the calculated mean value of nanoparticle concentration from two methods ICP-MS and weight loss.

The concentration values determined by both methods, as shown in Table 1, are in good agreement, which confirms the high stability of the colloids obtained and the lack of precipitation.

Table 1 Gold concentration in colloids from the analysis of ICP-MS measurements and weight loss

Sample	Average Au concentration from ICP-MS (mg L^{-1})	Average Au concentration from weight loss (mg L^{-1})
AuNPs-2	3.9 ± 0.5	4.4 ± 0.5
AuNPs-5	5.3 ± 0.6	6.3 ± 0.6

4. Conclusions

As shown by previous studies on electrical arc discharges between two gold electrodes in deionized water, controlled synthesis of gold nanoparticles in terms of different sizes and shapes is still a challenge. The present work shows the possibility of extending the syntheses of metal colloids with the method of conducting them in an alternating current arc. In contrast to DC methods, this process characterized by high voltage and low current, offers the possibility of obtaining smaller nanoobjects of oval shape, that are stable in water without stabilizing compounds. Gold nanoparticles were obtained using a very simple design of the supply system, which is feasible under common laboratory conditions. It was noticed that the longer the process, the larger the size of gold nanoparticles. During the arc discharge the surface lr of the Au electrodes was ablated and condensed *via* nucleation and coalescence processes in the water, creating a gold nanoparticles.

It was also noted that the use of alternating current evenly consumes the gold electrodes during the processes. Already from these preliminary results, it can be concluded that process parameters such as applied operating voltage, electric current, frequency, electrode shape and gap, water temperature are key factors in the production of nanoparticles. The chemical cleanliness of the water is a very important point. In further work, the presence of intentionally introduced contaminants in

the form of electrolytes or stabilizers will be thoroughly clarified. The process was carried out at room temperature, but in the future, these processes should be performed at constant water temperature in order to determine the influence of this factor on the formation of gold nanoparticles and other metallic nanostructures. No less important will be the explanation of the mechanism of stabilization of colloidal particles from the AC arc discharge process, which involves complex ion specific effects at the nanoparticle/water interface and is responsible for their long-term stability.

Data availability

The data that support the findings of this study are available from the corresponding author, Krzysztof Jankowski, upon request.

Conflicts of interest

The authors declare no conflict of interest. The results in the manuscript are original and the authors are fully responsible for their authenticity. The authors declare that this manuscript is our original work and that no part of it has been copied. The authors declare that the manuscript submitted to the RSC journal has not been published elsewhere and has not been simultaneously sent to other journals.

Acknowledgements

The purchase of a Malvern Panalytical Aeris powder X-ray diffractometer, on which XRD results were obtained, was funded by the EU Regional Operational Program of the Lodz Region, Poland, No. RPLD.01.01.00-10-0008/18.

References

1 J. Turkevich, P. C. Stevenson and J. Hillier, *Discuss. Faraday Soc.*, 1951, **11**, 55–75.
2 M. Brust, M. Walker, D. Bethell, D. J. Schiffrin and R. Whyman, *J. Chem. Soc., Chem. Commun.*, 1994, 801–802.
3 K. Aslan, J. Zhang, J. R. Lakowicz and C. D. Geddes, *J. Fluoresc.*, 2004, **14**, 391–400.
4 E. Pyrak, A. Jaworska and A. Kudelski, *Molecules*, 2019, **24**, 3921.
5 M. António, J. Nogueira, R. Vitorino and A. L. Daniel-da-Silva, *Nanomaterials*, 2018, **8**, 200.
6 A. Neeley, S. A. Khan, L. Beqa, Z. Fan, A. K. Singh, W. Lu, D. Senapati, T. Arbneshi, E. Lee and Y. Anderson, *IEEE Trans. Nanotechnol.*, 2010, **10**, 26–34.
7 M. S. Draz and H. Shafiee, *Theranostics*, 2018, **8**, 1985.
8 S. Jongjinakool, K. Palasak, N. Bousod and S. Teepoo, *Energy Procedia*, 2014, **56**, 10–18.
9 C. Chen, W. Liu, S. Tian and T. Hong, *Sensors*, 2019, **19**, 1712.
10 D. T. Thompson, *Nano Today*, 2007, **2**, 40–43.
11 D. Huang, F. Liao, S. Molesa, D. Redinger and V. Subramanian, *J. Electrochem. Soc.*, 2003, **150**, G412.
12 S. D. Perrault and W. C. Chan, *Proc. Natl. Acad. Sci. U. S. A.*, 2010, **107**, 11194–11199.
13 W. Zhou, X. Gao, D. Liu and X. Chen, *Chem. Rev.*, 2015, **115**, 10575–10636.
14 S. Alizadeh and Z. Nazari, *J. Chem. Rev.*, 2020, **2**, 228–242.
15 M. Wuithschick, A. Birnbaum, S. Witte, M. Sztucki, U. Vainio, N. Pinna, K. Rademann, F. Emmerling, R. Kraehnert and J. Polte, *ACS Nano*, 2015, **9**, 7052–7071.
16 M. Bardají, P. Uznanski, C. Amiens, B. Chaudret and A. Laguna, *Chem. Commun.*, 2002, 598–599.
17 P. Uznanski, C. Amiens, M. Bardaji, B. Donnadieu, Y. Coppel, B. Chaudret and A. Laguna, *New J. Chem.*, 2001, **25**, 1495–1499.
18 Y. Shang, C. Min, J. Hu, T. Wang, H. Liu and Y. Hu, *Solid State Sci.*, 2013, **15**, 17–23.
19 L. Freitas de Freitas, G. H. C. Varca, J. G. Dos Santos Batista and A. Benévolo Lugão, *Nanomaterials*, 2018, **8**, 939.
20 J. Fuentes-García, J. Santoyo-Salzar, E. Rangel-Cortes, G. F. Goya, V. Cardozo-Mata and J. A. Pescador-Rojas, *Ultrason. Sonochem.*, 2021, **70**, 105274.
21 M. K. Corbierre, J. Beerens and R. B. Lennox, *Chem. Mater.*, 2005, **17**, 5774–5779.
22 K. Bi, Y. Chen, Q. Wan, T. Ye, Q. Xiang, M. Zheng, X. Wang, Q. Liu, G. Zhang and Y. Li, *Nanoscale*, 2019, **11**, 1245–1252.
23 A. Lévy, M. De Anda Villa, G. Laurens, V. Blanchet, J. Bozek, J. Gaudin, E. Lamour, S. Macé, P. Mignon, A. R. Milosavljević, C. Nicolas, M. Patanen, C. Prigent, E. Robert, S. Steydli, M. Trassinelli, D. Vernhet, O. Veteläinen and D. Amans, *Langmuir*, 2021, **37**, 5783–5794.
24 H. Wender, M. L. Andreazza, R. R. Correia, S. R. Teixeira and J. Dupont, *Nanoscale*, 2011, **3**, 1240–1245.
25 A. A. Ashkarran, S. M. Mahdavi, M. M. Ahadian and M. R. Hormozi Nezhad, *Appl. Phys. A*, 2009, **96**, 423–428.
26 H. Ghomi, M. Yousefi, N. Shahabi and M. Khoramabadi, *Radiat. Eff. Defects Solids*, 2013, **168**, 881–891.
27 K.-H. Tseng, C.-Y. Liao, J.-C. Huang, D.-C. Tien and T.-T. Tsung, *Mater. Lett.*, 2008, **62**, 3341–3344.
28 D.-C. Tien, L.-C. Chen, N. Van Thai and S. Ashraf, *J. Nanomater.*, 2010, **2010**, 634757.
29 T. V. Verissimo, N. T. Santos, J. R. Silva, R. B. Azevedo, A. J. Gomes and C. N. Lunardi, *Mater. Sci. Eng. C*, 2016, **65**, 199–204.
30 I. Fratoddi, I. Venditti, C. Cametti and M. V. Russo, *Nano Res.*, 2015, **8**, 1771–1799.
31 N. Khlebtsov and L. Dykman, *Chem. Soc. Rev.*, 2011, **40**, 1647–1671.
32 A. Orlando, M. Colombo, D. Prosperi, F. Corsi, A. Panariti, I. Rivolta, M. Masserini and E. Cazzaniga, *J. Nanopart. Res.*, 2016, **18**, 1–12.
33 J.-K. Lung, J.-C. Huang, D.-C. Tien, C.-Y. Liao, K.-H. Tseng, T.-T. Tsung, W.-S. Kao, T.-H. Tsai, C.-S. Jwo and H.-M. Lin, *J. Alloys Compd.*, 2007, **434**, 655–658.
34 A. A. Ashkarran, *J. Theor. Appl. Phys.*, 2012, **6**, 1–6.
35 A. M. El-Khatib, M. S. Badawi, Z. Ghatass, M. Mohamed and M. Elkhatib, *J. Cluster Sci.*, 2018, **29**, 1169–1175.
36 S. Iijima, *Nature*, 1991, **354**, 56–58.

37 J. Jabłońska, K. Jankowski, M. Tomasik, D. Cykalewicz, P. Uznański, S. Całuch, M. Szybowicz, J. Zakrzewska and P. Mazurek, *SN Appl. Sci.*, 2021, **3**, 1–10.
38 K. Jankowski, A. Ostafin, M. Tomasik, T. Nyokong and J. Britton, *SN Appl. Sci.*, 2020, **2**, 1–6.
39 V. Amendola and M. Meneghetti, *J. Phys. Chem. C*, 2009, **113**, 4277–4285.